Materials Characterization 171 (2021) 110747

Contents lists available at ScienceDirect

Materials Characterization

journal homepage: www.elsevier.com/locate/matchar

Micromachining imposed subsurface plastic deformation in single-crystal aluminum

Sudhanshu Nahata [a,1], Marzyeh Moradi [b,2], Yoosuf N. Picard [a,b,*,3], Nithyanand Kota [a,4], O. Burak Ozdoganlar [a,b,c,*]

[a] Department of Mechanical Engineering, Carnegie Mellon University, Pittsburgh, PA 15213, USA
[b] Department of Material Science and Engineering, Carnegie Mellon University, Pittsburgh, PA 15213, USA
[c] Department of Biomedical Engineering, Carnegie Mellon University, Pittsburgh, PA 15213, USA

ARTICLE INFO

Keywords:
Aluminum
Subsurface plastic deformation
Micromachining
Shear bands
Recrystallized microstructure

ABSTRACT

Mechanical removal of metal induces deformation and changes to microstructural characteristics of the newly created surfaces. The mode and extent of deformation can be difficult to predict since it depends on the local crystallographic orientation, which varies significantly for polycrystalline metals. In this work, we analyzed the deformation mode and extent beneath machined surfaces of different crystallographic orientations. This was accomplished by orthogonal micromachining of single-crystal aluminum along six different crystallographic orientations orthogonal to the sample [111] zone-axis, followed by electron backscatter diffraction (EBSD) analysis to evaluate the resulting subsurface microstructure and crystal lattice rotation. The results indicate that differences in the initial material crystallographic orientation produce significant variations in the depth of deformation (compared to the uncut chip thickness), the degree of grain refinement and the extent of lattice rotations. We grouped the orientation as "hard" or "soft" based on the measured cutting force. The soft orientations exhibit deformation modes consisting of shear bands and lattice rotations; whereas hard orientations exhibit deformation modes consistent with strain hardening: localized dynamic recrystallization, highly entangled dislocations and minimal crystal lattice rotations. The depth of subsurface deformation for some orientations was extensive, reaching depths far greater than the uncut chip thicknesses. Overall, we conclude that the cutting force required to machine a given orientation does provide some insight on the local deformation mode, and orientations can be easier or harder to machine based on local susceptibility to shear and lattice rotation.

1. Introduction

Micromachining and ultraprecision machining (e.g., diamond turning) of polycrystalline metals often involves uncut chip thicknesses commensurate with the grain size of the workpiece material. At these scales, the material cannot be assumed to be isotropic, and hence, the local crystallographic orientation must be considered [1–9]. The quality of the end-products, including the surface finish [10–12] and material properties [13] of the cut-surface, strongly depend on the material removal behavior during machining. Machining operations deform the surface beneath the cut, thereby altering the material characteristics and mechanical properties of the newly created surface [14,15]. The degree of grain refinement beneath the cut-surface is critical in determining the hardness [16–18], residual stress [14,17] and wear properties [6,19,20] of the newly created surface. In addition, the deformation mode and the extent of subsurface deformation serves as a validation to models that predict the machining induced deformation and microstructure evolution [21–23]. Therefore, it is critical to characterize the extent and mode of deformation in crystalline metals as a function of local crystalline orientation.

Previously, the anisotropic behavior of single-crystal aluminum during orthogonal cutting has been analyzed, where large variations in

* Corresponding authors at: Department of Mechanical Engineering, Carnegie Mellon University, Pittsburgh, PA 15213, USA.
E-mail addresses: Yoosuf.Picard@netl.doe.gov (Y.N. Picard), ozdoganlar@cmu.edu (O.B. Ozdoganlar).
[1] Currently at ASML US, CT.
[2] Currently at KLA-Tencor, CA.
[3] Currently at National Energy Technology Laboratory, PA.
[4] Currently at Adobe Inc., CA.

https://doi.org/10.1016/j.matchar.2020.110747
Received 22 August 2020; Received in revised form 16 October 2020; Accepted 2 November 2020
Available online 5 November 2020

the thickness of (cut) chip and the shear angle were observed, indicating variation in deformation when cutting along different crystallographic orientations [24]. Cutting forces and surface roughness values were also observed to vary with the cutting direction even when the cutting plane is identical [10–12]. More recently, a semi-empirical model of the shear angle and specific energies for f.c.c. single-crystals was developed by integrating a crystal plasticity model with a machining model [25–27]. Furthermore, comprehensive experiments were conducted on single-crystal and coarse-grained aluminum under varying machining conditions to assess the crystal anisotropy using the analysis of variance approach [28,29].

Although most of the efforts in the past have been dedicated to understanding the effect of the material anisotropic behavior on machining responses, i.e., cutting force, shear angle and surface roughness, only a few studies have directly investigated the microstructural evolution and deformation mechanisms *beneath* the machined—newly created—surfaces. The material characteristics and the associated mechanical properties of the newly created surface is of utmost importance due to its effects on the performance of fabricated components. Of the handful of studies focused on understanding the machining induced [28,30,31] or wear induced deformations [32–34] in single-crystal materials, the analysis of single-crystal aluminum during diamond turning [31] showed the evolution of both simple shear and compression textures on the machined surfaces. The deformed region was seen to extend as much as 150 μm deep for an uncut chip thickness of 10 μm. In [30], transmission electron microscopy (TEM) was used to characterize depth of damage induced in single-crystal aluminum by single point diamond flycutting. Recently, Kota et al. [28] also conducted preliminary analysis on sub-surface deformation during orthogonal cutting of single-crystal aluminum, where microstructural changes could be detected up to 20 μm in depth for an uncut chip thickness of 20 μm. In [35], we presented a preliminary investigation of single crystal machining where we analyze the impact of cleanup cuts on machining forces and quantify misorientation as a function of subsurface depth for three different crystallographic orientations. Although, these studies provide an initial estimate of the machining induced deformations in single-crystal aluminum, the change in deformation behavior as a function of crystallographic directions has not been well characterized.

The variation in subsurface deformation with changing cutting directions for different cutting planes can provide critical insights on how deformation modes might vary. Those insights can be used for modeling polycrystalline workpieces during micromachining and precision machining, where, due to the small uncut chip thicknesses, the process is dominated by how cutting will vary based on individual grains with different orientations. However, to date, no study has comprehensively characterized the subsurface microstructure (i.e., recrystallization, lattice rotation, shear bands) after orthogonal machining single-crystal aluminum along various cutting orientations. Therefore, in this study, an orthogonal planing approach [28,35] was used to diamond cut single-crystal aluminum samples (see Fig. 1(a)) in conjunction with electron backscatter diffraction (EBSD) analysis in order to evaluate subsurface microstructure and associated deformation mode.

2. Material and Methods

The single-crystal aluminum samples, in the form of discs with 25.4 mm diameter and 1.8 mm thickness, were procured from Goodfellow USA. The disc center axis and face surface normal was parallel with the Al [111] zone-axis, and hence, all cutting planes and cutting directions lay perpendicular to the [111] direction, as shown in Fig. 1(b). The in-plane directions were confirmed (with better than 1 deg. resolution) by X-ray diffraction (XRD) using a Panalytical X'Pert Pro MRD X-ray Diffractometer. The sample was machined along eight different crystallographic directions using a single-crystal diamond tool at a 40 mm/s cutting speed (v) and 40 μm uncut chip thickness (a_0), as shown in Fig. 1(a). Out of eight machined orientations, six orientations, as labeled in Fig. 1(a), were studied in this work.[5] The diamond cutting tool has a 200 nm edge radius (measured by atomic force microscopy) with 0° rake and 60° clearance angle. The zero-degree rake angle tool was selected to study subsurface deformation as a reasonable medium between positive and negative rake angles.

Machining forces in cutting, thrust and lateral directions were measured using a Kistler 9256C2 3-axis dynamometer (see Fig. 2(a)). The force data at the onset and end of the cutting process were removed to eliminate possible boundary effects, and only the central portion was used during our analysis. The cut chips generated during machining for each orientation were collected and imaged using an optical microscope (Alicona G4 InfiniteFocus) to measure their thickness (see Fig. 2(b)). An average of three measurements along the length of each cut-chip (from a uniform section) are reported.

The machined sample was cold mounted in a conductive epoxy and the Al (111) disc face was mechanically polished (mirror finish) to enable EBSD analysis. The sample was analyzed in a FEI Quanta 200 field emission gun (FEG) scanning electron microscope (SEM) equipped with EDAX EBSD system using a Hikari CCD camera. A hexagonal grid was used to collect EBSD data points at 4 × 4 camera binning with 15 kV SEM acceleration voltage and 5.5 nA SEM probe current. A neighbor confidence index (CI) correlation method was employed to clean-up the EBSD data. The EBSD scan areas spanned the machined edge towards the center (undeformed region) in order to assess the extent and mode of subsurface deformation caused by machining.

Prior to machining, multiple clean-up cuts of 4 μm (10% of the target uncut chip thickness) were made, with depths twice the previous largest cut for each cutting direction to remove any residual deformation due to the previous cuts. Fig. 1(c) presents EBSD-acquired inverse pole figures (IPF) for a sample after clean-up cut (or before machining) and after machining. Based on the results, the deformation prior to machining is assumed to be negligible with respect to the uncut chip thickness of 40 μm.

The extent and the mode of subsurface deformation as a function of crystallographic orientation was explored by EBSD through inverse pole figures (IPF), pole figures, misorientation angle line profiles and kernel average misorientation (KAM) maps. Since machining forces and cut-chip thicknesses were also measured during orthogonal cutting, these served as additional metrics which are useful for comparing deformation and plasticity behavior for different cutting orientations. Therefore, these metrics are presented prior to any discussions.

3. Results and Discussion

Fig. 2(c)–(d) presents cutting and thrust force magnitudes recorded during machining, which is averaged over the length of the cut; the error bars indicate the full-range about the calculated average. The measured chip thicknesses were used to calculate the shear angles (φ, see Fig. 2(e)) with a thin-shear-plane approximation by taking the ratio of measured chip thickness before and after the cut as

$$tan(\varphi) = \frac{\frac{a_o}{a_c} cos(\alpha)}{1 - \frac{a_o}{a_c} sin(\alpha)}, \quad (1)$$

where a_o and a_c are the uncut chip thickness and the measured cut-chip thickness, respectively, and α is the tool rake angle. It is noted that the deformation mechanism in single-crystal ductile metal machining is rather complex and typically involves incremental calculation of plastic work [26,27] and/or shear stress [2] in the active slip systems. Considering the machining parameters used and the observed microstructures, any modeling/analytical prediction should consider latent hardening and the formation of grain boundaries. Such modeling/

[5] The remaining two orientations did not provide useful data since the signal-to-noise ratios in cutting forces and orientation maps were too low.

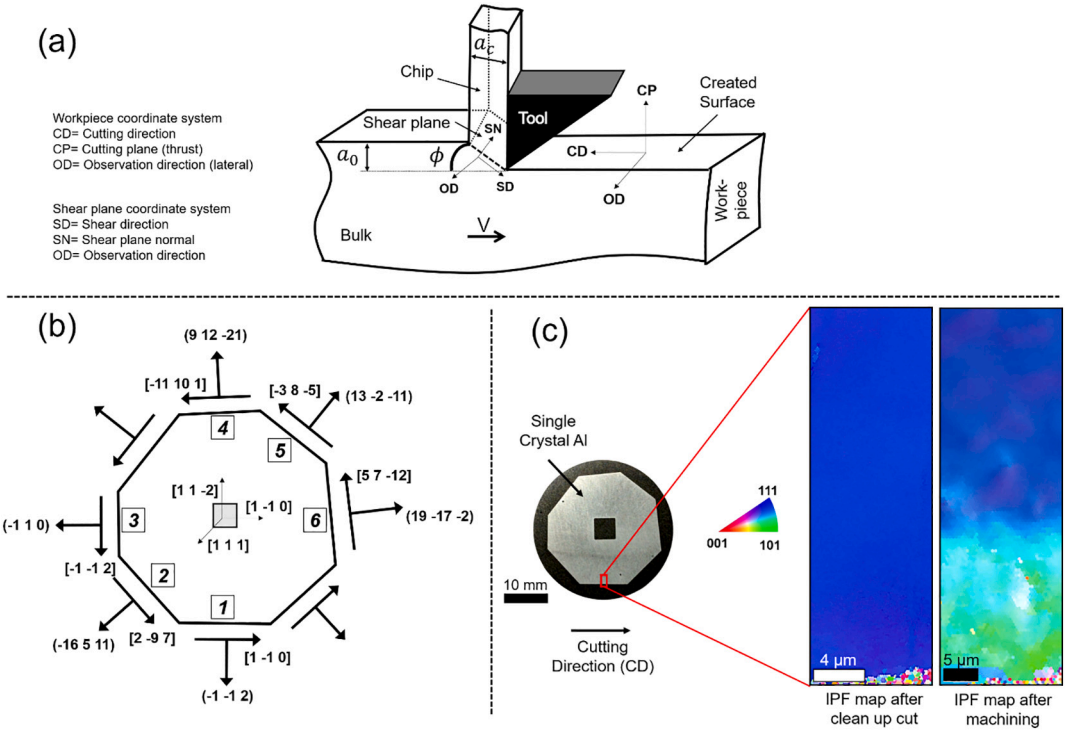

Fig. 1. (a) Illustration of the orthogonal planing configuration with a 0 deg. rake angle tool, (b) schematic outlining the six orthogonal planing conditions relating the single-crystal aluminum sample orientation with respect to the cutting planes and directions, and (c) composite image presenting a photograph of the specimen with a highlighted region used for EBSD analysis with inverse pole figure (IPF) maps after clean-up cutting (or before machining) and after machining. The EBSD maps are built along the observation direction (OD).

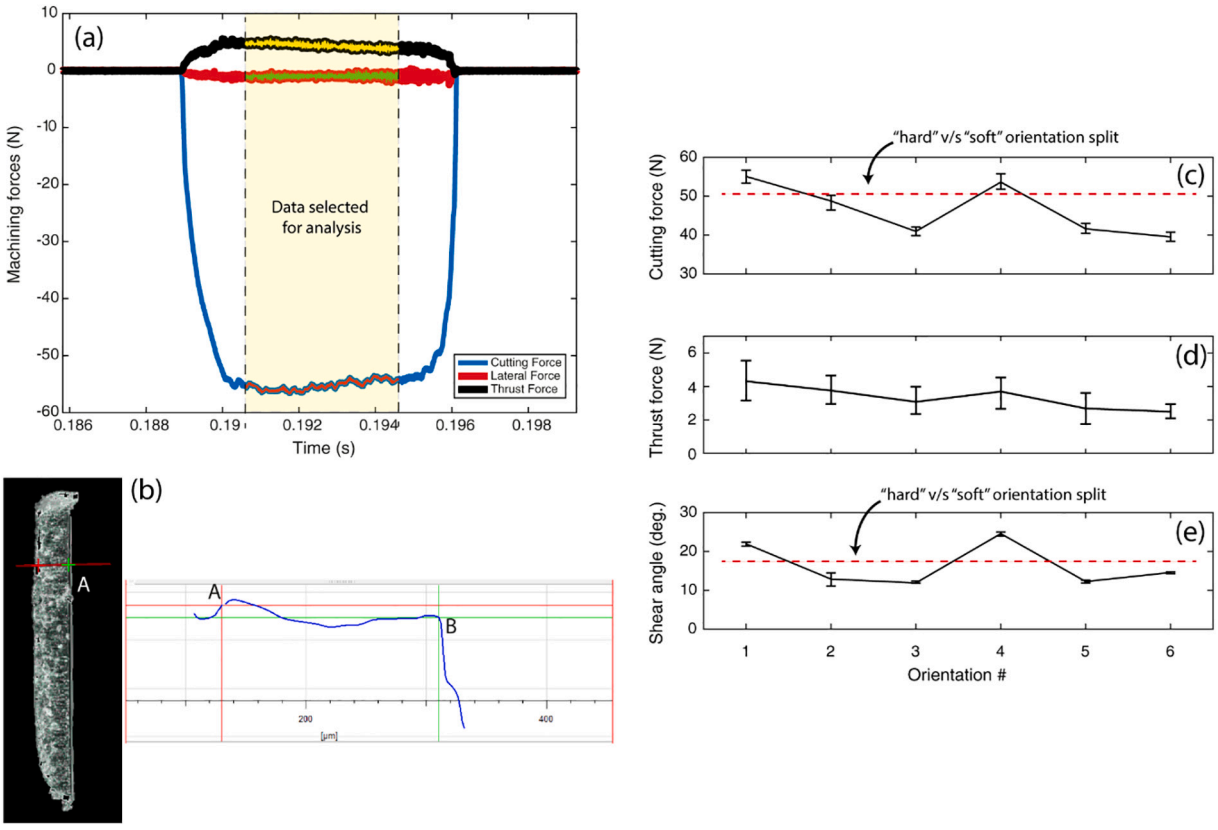

Fig. 2. (a) Example force data measured during orthogonal micromachining and (b) example optical micrograph of a cut-chip for thickness measurement. Experimental and calculated micromachining data plotted as a function of the six sample orientations: (c) cutting forces along the direction of cut F_c, (d) thrust forces perpendicular to the direction of cut F_t, (e) shear angle φ.

analytical efforts are outside of the scope of this work. Taylor factor (TF) was not applicable due to the observation of near-surface crystal lattice rotations for some orientations.

From Fig. 2(c)–(e), the cutting and thrust forces, and the shear angle were seen to vary with the crystallographic orientations, confirming the anisotropic nature of micromachining a single-crystal metal. These variations are used to group the orientations in order to compare deformation behavior to measured cutting forces (presented later in the text). An arbitrary split was made at 50 N cutting force where the higher cutting force orientations 1 and 4 are termed "hard" orientations and the rest of the orientations are termed "soft" orientations (see Fig. 2(c)). This grouping of hard/soft orientations by higher/lower cutting force is also consistent with higher/lower calculated shear angles.

IPF maps and pole orientations of the subsurface region for the six micromachined orientations are presented in Fig. 3, where [111] direction is consistently out-of-plane. The pole figures are generated from a larger IPF image than shown (depth > 60 μm). The bottom edge is identified as the machined surface for all IPF maps in Fig. 3(a), and the direction of machining is from left to right. For soft orientations, machining was seen to cause noticeable counter-clockwise crystal lattice rotations about [111], which are also observed as the counter-clockwise (CCW) smearing of ⟨111⟩ poles in the corresponding pole figures in Fig. 3(b).

Pole figures for the "hard" orientations 1 and 4 do not show appreciable smearing of the ⟨111⟩ poles, indicating negligible crystal lattice rotations. For orientation 1, the out-of-plane direction changes from [101] to [111] at an approximately 10 μm depth. Given that the rotation about [111] pole is negligible, the deformation is expected to diminish beyond ~10 μm subsurface. Therefore, in hard orientations (i.e., 1 and 4), the plastic deformation does not penetrate as deep into the material subsurface as extensively as the "soft" orientations, where appreciable crystal lattice rotations are observed. In all cases, dynamic recrystallization occurred up to a depth of ~10 μm based on the observation of polycrystalline grains formed at the machined near-surfaces. Likewise, in single-point diamond flycutting of Al single-crystals [30], evidence of crystal growth was observed by TEM only up to 3.2 μm below the {111} surface orientation for a 6 μm uncut chip thickness. The depth of damage was also reported to be a function of the cutting plane.

From Fig. 3(b), orientations 3 and 6 show significantly higher crystal lattice rotations than the other orientations, noticeable from the counter-clockwise rotation about the out-of-plane ⟨111⟩ direction. Specifically, orientation 6 exhibits ~50% lattice rotation while also experiencing the lowest forces during cutting (from Fig. 2(c)). A large out-of-plane lattice rotation could facilitate machining by presenting an easier-to-shear orientation to the tool, thereby producing a low cutting force and substantial subsurface deformation (high shear strain). Such counter-clockwise lattice rotations and formation of new grains were also observed in the molecular dynamics simulation of polycrystalline copper during microcutting [23]. Tilting of the cutting plane normal (equivalent to out-of-plane rotations in our case) has also been observed in previous sliding wear experiments [20]. While outside of the scope of this study, observed small-grain recrystallization at the machined surface for orientations 2 and 4 may produce higher hardness consistent with the Hall-Petch relationship [36]. Orientation 1 is unique in the sense that it shows a large grain formation across the whole machined surface, which is uncharacteristic of all other orientations.

Fig. 4(a) plots misorientation angle as a function of distance from the machined edge, where local orientation is referenced to the non-deformed bulk (111) surface far away (>60 μm) from the machined edge. An average of 10 different line measurements were taken to produce misorientation profiles. There are three distinct orientation pairs to note. Orientations 3 and 6 exhibit the largest degree of misorientations over the greatest depths subsurface. Orientations 2 and 5 exhibit moderate misorientations that do not extend as far as orientations 3 and 6. Meanwhile, orientations 1 and 4 show the highest degree of misorientations within the first 10 μm from the machined edge, but the misorientations decrease substantially beyond this depth to angles lower than those for the other orientations. These observations further substantiate the strong degree of localized dynamic recrystallization that appears to be characteristic for the "hard" orientations.

Fig. 4(b) presents KAM maps of the subsurface regions for all six machined edges. For orientation 1 and 4, KAM activity visible in the upper half of the maps are artifacts from mechanical polishing during specimen preparation. It should be noted that these artifacts do not influence observations from the IPF maps, pole figures, or misorientation profiles previously discussed.

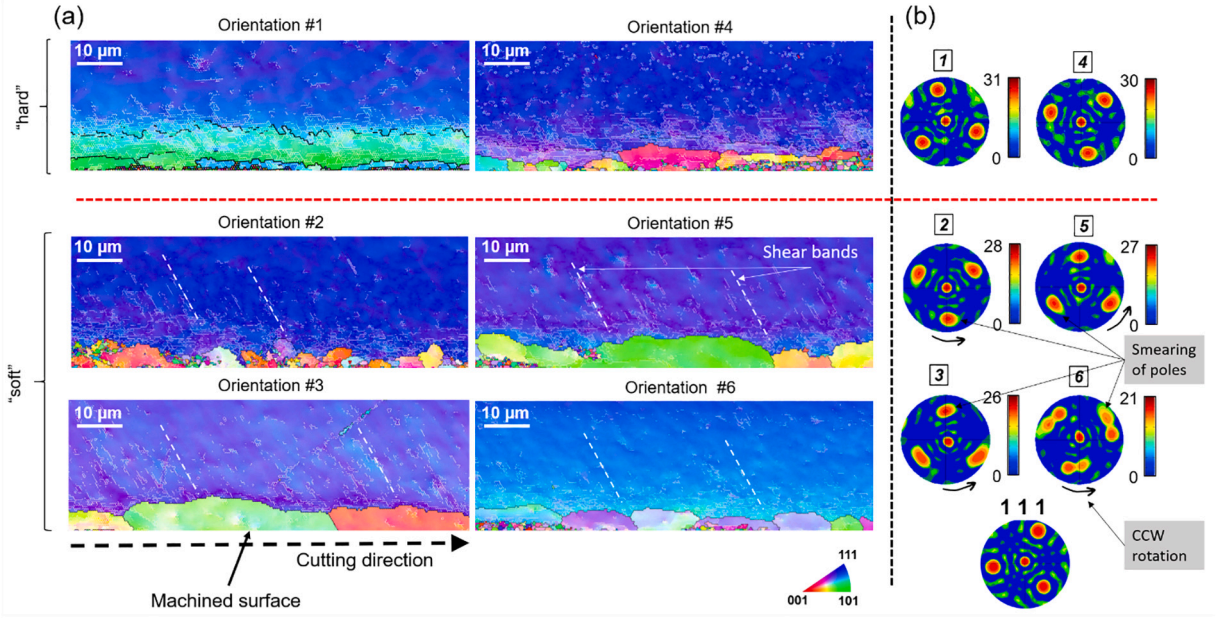

Fig. 3. (a) IPF maps of cross-sectioned, machined surfaces for six different orientations, where machining direction is from left to right, (b) pole figures for all six orientations as well as a reference for bulk, non-deformed case (bottom). Black lines are high angle [$\theta > 15^{\circ}$] grain boundaries and white lines are low angle [$2^{\circ} < \theta < 15^{\circ}$] grain boundaries. Dashed white lines indicate shear bands. The EBSD maps are built along the observation direction (OD).

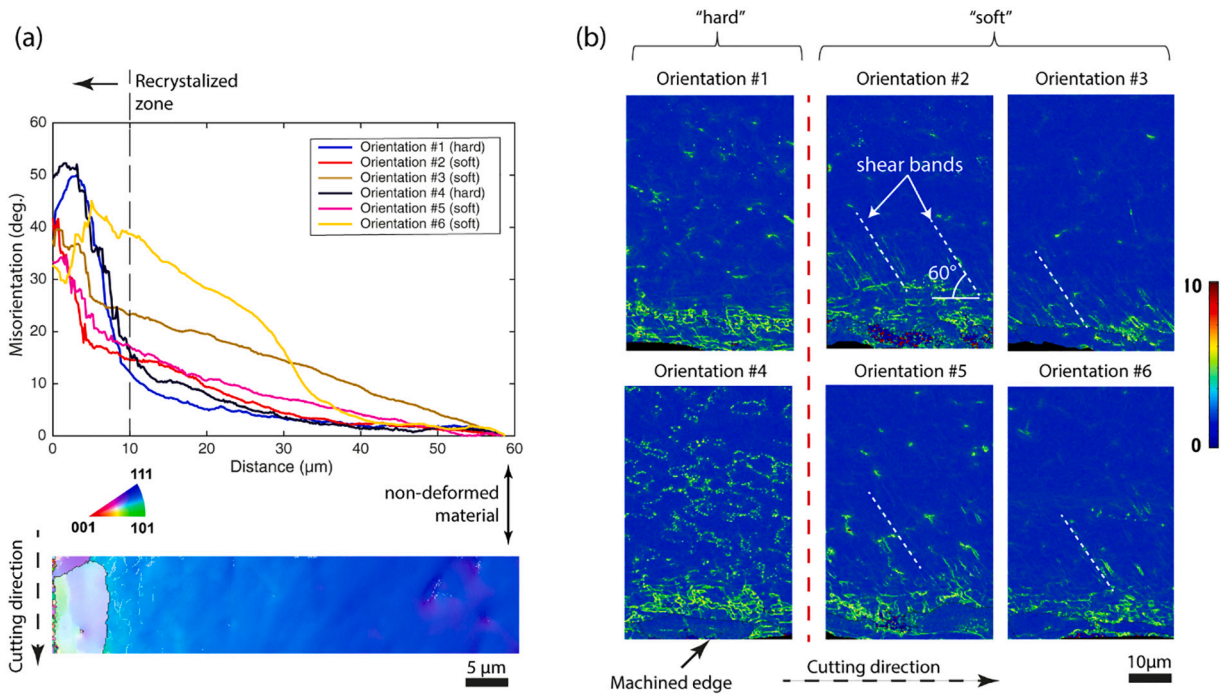

Fig. 4. (a) Point-to-origin misorientation angle, where origin is the bulk (non-deformed) region, and (b) kernel average misorientation (KAM), for orientations 1 to 6. The EBSD maps are built along the observation direction (OD).

Both the IPF maps and KAM maps for soft orientations 2, 3, 5 and 6 show the presence of shear bands- region of concentrated plastic flow- 5 to 30 μm beneath the machined surfaces. These shear bands extend to the depths of 20–30 μm for an uncut chip thickness of 40 μm and are oriented between 55° and 60° to the horizontal direction. Among those, orientation 2 and 5 show shear banding with little lattice rotations when compared to orientations 3 and 6 that show shear banding with large lattice rotations. This reveals slightly different deformation modes for the "soft" orientations. During sliding wear of single-crystal Al, slip shear bands were oriented at 55° with respect to the sliding direction [34]. Equal channel angular pressing (ECAP) of single-crystal Al also resulted in a shear band formation after 60° counter-clockwise rotation about the [112] axis to a crystal orientation parallel to the (111) slip plane, thus a "soft" shearing direction [37]. Furthermore, shear bands were observed at 60° for (111)[$\bar{2}$11] (orientation 3 in our study), but not for (111)[$\bar{1}$10] (orientation 1 in our study) during a molecular dynamics (MD) simulation of nanometric cutting of single-crystal Al [6]. For orientations 1 and 4, where the shear bands are absent, the KAM maps indicate higher density dislocations and more entangled dislocation formation at a more confined depth than other orientations, confirming a strain hardening mechanism is tied to the "hard" orientations.

In general, the total deformation of the material can be expressed as a sum of shear strain and rigid body rotation [38]. The shear strain results in a greater amount of work hardening (seen for "hard" orientations), compared to lattice rotation (seen for "soft" orientations). More specifically, the plastic deformation during orthogonal machining process can be described as a combination of compression and shear deformation ahead of the tool along the cutting direction [2]. According to MD simulation by [39], the strain rate did not demonstrate considerable effects on the mechanical properties and elastic-plastic deformation of the material for both tension and compression. Therefore, the impact of cutting speed on resulting deformation modes is expected to be insignificant.

As noted before, the deformation mechanism for orthogonal machining of single-crystal ductile metals is difficult to model and therefore needs extensive experimental results for verification. Crystal Plasticity FEM (CPFEM) [40–43] is commonly used as an approach to investigate deformation mechanisms in severe plastic deformation processes such as Accumulative Roll Bonding (ARB), ECAP and high pressure torsion. Traditionally, for orthogonal cutting, researchers have modeled the resulting cutting forces, chip morphology and in some cases, orientation changes. CPFEM would benefit from additional experimental data to validate existing models. The work provided in this study may prove useful towards validating existing deformation models. Future work with CPFEM should be able to predict what combination of recrystallization, strain hardening and crystal lattice rotation can be expected for a given crystal orientation, thereby providing critical information for predicting surface hardness and wear resistance for machined metal surfaces.

4. Conclusions

In summary, plastic deformation caused by the orthogonal micromachining resulted in significant changes (in relation to uncut chip thickness) in the microstructure beneath the newly created surface. Furthermore, the extent and mode of deformation is strongly dependent on the crystallographic orientation. The main conclusions are: (1) for the machined orientations, cutting forces sees a significant variation between different crystallographic orientations about the [111] zone axis which is expected from the anisotropic nature of single crystals. (2) The softer orientations (2,3,5 and 6) show higher out-of-plane lattice rotations and therefore, higher effective strains— resulting in larger overall deformation—as compared to hard orientations (1 and 4). This is further confirmed by examining the misorientation plots, where the deformation extends to higher depths for softer orientations than the harder orientations. The softer orientations also show deformation mode by slip and shear bands that are non-existent for hard orientations. (3) On the other hand, hard orientations show minimal out-of-plane lattice rotations and demonstrate localized dynamic recrystallization that is confined within a smaller depth from the machined surface as compared to soft orientations.

Data Availability

The data that support the findings of this study are available from the corresponding author upon reasonable request.

Declaration of Competing Interest

The authors declare that they have no known competing financial interests or personal relationships that could have appeared to influence the work reported in this paper.

Acknowledgements

The authors are grateful to Tom Nuhfer of Material Characterization Facility at Carnegie Mellon University for his help during the EBSD scans. The authors acknowledge use of the Materials Characterization Facility at Carnegie Mellon University supported by grant MCF-677785.

References

[1] S. Abolfazl Zahedi, M. Demiral, A. Roy, V.V. Silberschmidt, FE/SPH modelling of orthogonal micro-machining of f.c.c. single crystal, Comput. Mater. Sci. 78 (2013) 104–109, https://doi.org/10.1016/j.commatsci.2013.05.022.
[2] S. Abolfazl Zahedi, A. Roy, V.V. Silberschmidt, Variation of cutting forces in machining of f.c.c. single crystals, Acta Mech. 227 (2016) 3–9, https://doi.org/10.1007/s00707-015-1418-z.
[3] B.L. Lawson, N. Kota, O.B. Ozdoganlar, Effects of crystallographic anistropy on orthogonal micromachining of single-crystal aluminum, J. Manuf. Sci. Eng. 130 (2008), https://doi.org/10.1115/1.2917268.
[4] M. SATO, Y. KATO, S. AOKI, A. IKOMA, Effects of crystal orientation on the cutting mechanism of the aluminum single crystal: 2nd report: on the (111) plane and the (112) end cutting, Bull. JSME 26 (1983) 890–896, https://doi.org/10.1299/jsme1958.26.890.
[5] W.B. Lee, M. Zhou, A theoretical analysis of the effect of crystallographic orientation on chip formation in micromachining, Int. J. Mach. Tools Manuf. 33 (1993) 439–447, https://doi.org/10.1016/0890-6955(93)90050-5.
[6] R. Komanduri, N. Chandrasekaran, L.M. Raff, MD simulation of indentation and scratching of single crystal aluminum, Wear 240 (2000) 113–143, https://doi.org/10.1016/S0043-1648(00)00358-6.
[7] P.H. Cohen, The Orthogonal In-Situ Machining of Single and Polycrystalline Aluminum and Copper, The Ohio State University, 1982.
[8] A. Sharma, D. Datta, R. Balasubramaniam, Molecular dynamics simulation to investigate the orientation effects on nanoscale cutting of single crystal copper, Comput. Mater. Sci. 153 (2018) 241–250, https://doi.org/10.1016/j.commatsci.2018.07.002.
[9] N. Jia, P. Eisenlohr, F. Roters, D. Raabe, X. Zhao, Orientation dependence of shear banding in face-centered-cubic single crystals, Acta Mater. 60 (2012) 3415–3434, https://doi.org/10.1016/j.actamat.2012.03.005.
[10] K. Ueda, K. Iwata, K. Nakayama, Chip formation mechanism in single crystal cutting of β-brass, CIRP Ann. Manuf. Technol. 29 (1980) 41–46, https://doi.org/10.1016/S0007-8506(07)61292-X.
[11] S. To, W.B. Lee, C.Y. Chan, Ultraprecision diamond turning of aluminium single crystals, J. Mater. Process. Technol. 63 (1997) 157–162, https://doi.org/10.1016/S0924-0136(96)02617-9.
[12] M. Zhou, B.K.A. Ngoi, Effect of tool and workpiece anisotropy on microcutting processes, Proc. Inst. Mech. Eng. Part B J. Eng. Manuf. 125 (2001) 13–19, https://doi.org/10.1243/0954405011515091.
[13] S. To, W.B. Lee, Deformation behaviour of aluminium single crystals in ultraprecision diamond turning, J. Mater. Process. Technol. 113 (2001) 296–300, https://doi.org/10.1016/S0924-0136(01)00667-7.
[14] Z. Pan, Y. Feng, S.Y. Liang, Material microstructure affected machining: a review, Manuf. Rev. 4 (2017) 5, https://doi.org/10.1051/mfreview/2017004.
[15] L. Zhang, H. Huang, H. Zhao, Z. Ma, Y. Yang, X. Hu, The evolution of machining-induced surface of single-crystal FCC copper via nanoindentation, Nanoscale Res. Lett. 8 (2013) 211, https://doi.org/10.1186/1556-276x-8-211.
[16] C.H. Che-Haron, A. Jawaid, The effect of machining on surface integrity of titanium alloy Ti-6% Al-4% V, J. Mater. Process. Technol. 166 (2005) 188–192, https://doi.org/10.1016/j.jmatprotec.2004.08.012.
[17] A. Yamamoto, T. Yamada, S. Nakahigashi, L. Liu, M. Terasawa, H. Tsubakino, Effects of surface grinding on hardness distribution and residual stress in low carbon austenitic stainless steel SUS316L, ISIJ Int. 44 (2004) 1780–1782, https://doi.org/10.2355/isijinternational.44.1780.
[18] D. Zhang, X.M. Zhang, J. Leopold, H. Ding, Subsurface deformation generated by orthogonal cutting: analytical modeling and experimental verification, J. Manuf. Sci. Eng. Trans. ASME 139 (2017), 094502, https://doi.org/10.1115/1.4036994.
[19] N. Irani, L. Nicola, Modelling surface roughening during plastic deformation of metal crystals under contact shear loading, Mech. Mater. 132 (2019) 66–76, https://doi.org/10.1016/j.mechmat.2019.02.007.
[20] D.R. Wheeler, D.H. Buckley, Texturing in metals as a result of sliding, Wear 33 (1975) 65–74, https://doi.org/10.1016/0043-1648(75)90224-0.
[21] J.R. Michael, S.V. Prasad, J.M. Jungk, M.J. Cordill, D.J. Bammann, C.C. Battaile, N. R. Moody, B.S. Majumdar, Modeling of Friction-induced Deformation and Microstructures, Sandia National Laboratories, 2006.
[22] Q. Liu, A. Roy, S. Tamura, T. Matsumura, V.V. Silberschmidt, Micro-cutting of single-crystal metal: finite-element analysis of deformation and material removal, Int. J. Mech. Sci. 118 (2016) 135–143, https://doi.org/10.1016/j.ijmecsci.2016.09.021.
[23] S. Shimada, N. Ikawa, H. Tanaka, J. Uchikoshi, Structure of micromachined surface simulated by molecular dynamics analysis, CIRP Ann. Manuf. Technol. 43 (1994) 51–54, https://doi.org/10.1016/S0007-8506(07)62162-3.
[24] M. Sato, Y. Kato, K. Tsutiya, Effects of crystal orientation on the flow mechanism in cutting aluminum single crystal, Trans. Japan Inst. Met. 20 (1979) 414–422, https://doi.org/10.2320/matertrans1960.20.414.
[25] N. Kota, O.B. Ozdoganlar, A model-based analysis of orthogonal cutting for single-crystal FCC metals including crystallographic anisotropy, Mach. Sci. Technol. 14 (2010) 120–127, https://doi.org/10.1080/10910340903586517.
[26] N. Kota, A.D. Rollett, O.B. Ozdoganlar, A rate-sensitive plasticity-based model for machining of fcc single-crystals - part 1 : model development, J. Manuf. Sci. Eng. 133 (2011), 031017, https://doi.org/10.1115/1.4004134.
[27] N. Kota, A.D. Rollett, O. Burak, A rate-sensitive plasticity-based model for machining of fcc single-crystals – part 2 : model calibration and validation, J. Manuf. Sci. Eng. 133 (2011), 031018, https://doi.org/10.1115/1.4004135.
[28] N. Kota, O.B. Ozdoganlar, Orthogonal machining of single-crystal and coarse-grained aluminum, J. Manuf. Process. 14 (2012) 126–134, https://doi.org/10.1016/j.jmapro.2012.01.002.
[29] S. Nahata, N. Kota, O.B. Ozdoganlar, Micromachining of coarse-grained aluminum including crystallographic effects, J. Manuf. Process. 57 (2020) 600–613, https://doi.org/10.1016/j.jmapro.2020.06.034.
[30] J. Carr, C. Narayan, J. Kim, Single Point Diamond Machining Induced Damage on Single Crystal Copper, Aluminum and Gold, in: Proc. 6th ASPE Annu. Conf., St. Fé, NM, USA, 1991, pp. 96–99.
[31] S. To, W.B. Lee, C.F. Cheung, Orientation changes of aluminium single crystals in ultra-precision diamond turning, J. Mater. Process. Technol. 140 (2003) 346–351, https://doi.org/10.1016/S0924-0136(03)00756-8.
[32] S.Y. Tarasov, D.V. Lychagin, A.V. Chumaevskii, Orientation dependence of subsurface deformation in dry sliding wear of Cu single crystals, Appl. Surf. Sci. 274 (2013) 22–26, https://doi.org/10.1016/j.apsusc.2013.02.018.
[33] A.V. Chumaevskii, S.Y. Tarasov, D.V. Lychagin, Plastic strain arrangement in copper single crystals in sliding, in: AIP Conf. Proc, AIP, 2014, pp. 91–94.
[34] C.S. Tiwary, J. Prakash, S. Chakraborty, D.R. Mahapatra, K. Chattopadhyay, Subsurface deformation studies of aluminium during wear and its theoretical understanding using molecular dynamics, Philos. Mag. 98 (2018) 2680–2700, https://doi.org/10.1080/14786435.2018.1502481.
[35] S. Nahata, Y.N. Picard, N. Kota, O. Burak Ozdoganlar, Experimental investigation of sub-surface deformation using EBSD in single crystal aluminum during orthogonal micromachining, Microsc. Microanal. 20 (2014) 1472–1473, https://doi.org/10.1017/s143192761400909x.
[36] H. Fujita, T. Tabata, The effect of grain size and deformation sub-structure on mechanical properties of polycrystalline aluminum, Acta Metall. 21 (1973) 355–365, https://doi.org/10.1016/0001-6160(73)90191-0.
[37] Y. Fukuda, K. Oh-ishi, M. Furukawa, Z. Horita, T.G. Langdon, The application of equal-channel angular pressing to an aluminum single crystal, Acta Mater. 52 (2004) 1387–1395.
[38] C.N. Reid, Deformation Geometry for Materials Scientists, Pergamon Press, New York, 1973, https://doi.org/10.1016/c2013-0-02546-7.
[39] R. Rezaei, H. Tavakoli-Anbaran, M. Shariati, Mechanical characteristics and failure mechanism of nano-single crystal aluminum based on molecular dynamics simulations: strain rate and temperature effects, J. Solid Mech. 9 (2017) 794–801.
[40] P. Wei, C. Lu, H. Liu, L. Su, G. Deng, K. Tieu, Study of anisotropic plastic behavior in high pressure torsion of aluminum single crystal by crystal plasticity finite element method, Crystals 7 (2017) 362, https://doi.org/10.3390/cryst7120362.
[41] M. Liu, S. Nambu, T. Koseki, K.A. Tieu, K. Zhou, Three-dimensional quantification of texture heterogeneity in single-crystal aluminium subjected to equal channel angular pressing, Philos. Mag. 97 (2017) 799–819, https://doi.org/10.1080/14786435.2017.1282179.
[42] Q. Luan, H. Xing, J. Zhang, J. Jiang, Experimental and crystal plasticity study on deformation bands in single crystal and multi-crystal pure aluminium, Acta Mater. 183 (2020) 78–92, https://doi.org/10.1016/j.actamat.2019.11.006.
[43] H. Wang, C. Lu, K. Tieu, G. Deng, P. Wei, Y. Liu, A crystal plasticity FEM study of through-thickness deformation and texture in a {112}⟨111⟩ aluminium single crystal during accumulative roll-bonding, Sci. Rep. 9 (2019) 1–13, https://doi.org/10.1038/s41598-019-39039-y.